Drug Design, Development and Therapy

Dovepress
open access to scientific and medical research

Open Access Full Text Article

ORIGINAL RESEARCH

Preliminary study on conjugation of formononetin with multiwalled carbon nanotubes for inducing apoptosis via ROS production in HeLa cells

This article was published in the following Dove Press journal:
Drug Design, Development and Therapy

Bohong Guo
Cancheng Liao
Xiaohong Liu
Jun Yi

Department of Pharmaceutics, Guangdong Pharmaceutical University, Guangzhou, China

Background: The present work was conducted to prepare and evaluate multiwalled carbon nanotube–formononetin (MWCNT-FMN) composite for sustained delivery and inducing apoptosis via reactive oxygen species (ROS) production in HeLa cells.

Methods: The composite was prepared by solution mixing with short carboxylic group-functionalized multiwalled carbon nanotubes (MWCNT-COOH). Then the composite was characterized by laser particle size analysis, Fourier transform infrared spectrometry, X-ray diffractometry, differential scanning calorimetry, and scanning electron microscopy. Drug release rates in vitro were determined by dialysis method. The in vitro cytotoxicity study was performed using water soluble tetrazolium assay. The cellular apoptosis assay, ROS, and mitochondrial membrane potential (MMP) of HeLa cells were investigated by acridine orange and ethidium bromide double dye, 2′,7′-dichlorodihydrofluorescein diacetate, and 5,5′,6,6′-tetrachloro-1,1′,3,3′-tetraethyl-imidacarbocyanine iodide probe, respectively.

Results: The entrapment efficiency was 28.77%±0.15%, and the loading capacity was 12.05%±0.20%. The release of MWCNT-FMN was sustained, and the cumulative release rate of formononetin (FMN) from MWCNT-COOH was higher at pH 7.4 than at pH 5.3. The in vitro cytotoxicity assay demonstrated that FMN, MWCNT-COOH, and MWCNT-FMN had no significant effects on the proliferation and viability of mouse fibroblast 3T3 cells over 48 hours, while the cell growth inhibition of the three samples showed concentration-dependent for HeLa cells. Biological assay suggested FMN and MWCNT-FMN could induce apoptosis in HeLa cells, meanwhile the cells exhibited stronger ROS signal and more depolarized MMP than that of the control group.

Conclusion: These results preliminarily demonstrated that MWCNT-FMN exerted anticancer efficacy through cellular apoptosis induced by ROS-mediated mitochondrial dysfunctions in HeLa cells.

Keywords: multiwalled carbon nanotube, characterization, cytotoxicity, formononetin, apoptosis

Introduction

Formononetin (FMN; 7-hydroxy-4′-methoxyisoflavone) is an *O*-methylated isoflavone phytoestrogen and is a bioactive component found in red clover plants. Previous studies have shown that FMN inhibits tumor cell proliferation, migration, and invasion; induces apoptosis in breast, prostate, and cervical cancers, and osteosarcoma cell lines; and attenuates osteoclastogenesis.[1–5] However, it has serious side effects in clinical administration because of its poor hydrosolubility.[6] Therefore, it is necessary to find a suitable delivery system for the entrapment of FMN. A novel class of nanomaterial called carbon nanotube (CNTs) was discovered in 1991 via an arc-discharge

Correspondence: Bohong Guo
Department of Pharmaceutics, Guangdong Pharmaceutical University, 280 East Waihuan Road, Guangzhou Higher Education Mega Center, Guangzhou, 510006, China
Tel +86 20 3935 2117
Fax +86 20 3935 2129
Email guobohong@gdpu.edu.cn

submit your manuscript | www.dovepress.com
Dovepress
http://dx.doi.org/10.2147/DDDT.S169767

method.[7] Ever since their emergence as a nanotechnology, they have been assessed as candidates for targeted drug delivery because of their high aspect ratio and surface area, high mechanical strength, and ease of drug loading via π–π stacking interactions.[8,9] Many possible uses for CNTs can be found in the literature, such as drug delivery, cancer therapy,[10] thermal therapy, and tissue-targeted therapy.[11] In short, CNTs have many unique physical, chemical, and biological properties and they have been extensively explored for biological and medical applications.[12,13] However, pristine CNTs are intrinsically insoluble in an aqueous medium and tend to aggregate into bundles caused by their highly hydrophobic surfaces, low functionality, and large size, coupled with van der Waals forces and strong π–π interactions between the individual tubes. Consequently, CNTs have poor biocompatibility and high toxicity.[14–16] Therefore, it is crucial to modify CNTs through covalent or noncovalent functionalization of their external walls in order to improve their dispersion and stability, rendering them to be more biocompatible and less toxic. Functional CNTs can demonstrate improved properties for drug delivery including increased solubility, selectivity, blood circulation time, and uptake and accumulation within tumor cells.[17] Ren et al acidized raw multiwalled CNTs (MWCNT) to obtain oxidized MWCNT (OX-MWCNT) and found that OX-MWCNT can not only be distributed in the brain but also accumulate in tumors[18] and have an ultra-high surface area for remarkably high loading of anticancer drugs. Razzazan et al purified pristine single-walled CNT (SWCNT) to acquire high purity SWCNT in order to produce nanotubes with available sidewalls to easily covalently conjugate drug.[19] Mehra et al have demonstrated that CNTs with an engineered surface can easily cross the blood–brain barrier without requiring any external transporter devices, owing to their nanosize and tiny nanoneedle tubular structure morphology.[11] Several studies have demonstrated that CNTs could be used to treat a variety of diseases, including cancer and chronic infections.[20–23] Consequently, in the current study we have chosen to investigate the potential of carboxylic group-functionalized multiwalled carbon nanotubes (MWCNT-COOH) as a drug carrier.

The aim of this work was to develop a suitable delivery system for the entrapment of FMN. Laser particle size analysis, Fourier transform infrared spectrometry (FTIR), differential scanning calorimetry (DSC), X-ray diffractometry (XRD), and scanning electron microscopy (SEM) were used to characterize multiwalled carbon nanotube–formononetin (MWCNT-FMN) conjugates. In order to evaluate the cytotoxicity in healthy cells and the anticancer activity of the free drug and nanocomposites, in vitro cytotoxicity studies were performed using 3T3 cells and HeLa cells for a treatment period of 48 hours. Additionally, the cellular apoptosis assay, reactive oxygen species (ROS), and mitochondrial membrane potential (MMP) of HeLa cells were studied to learn about the mechanism of apoptosis.

Materials and methods

Materials

MWCNT-COOH (>95% purity, diameter 20–30 nm, length 0.5–2 μm) was produced by Chengdu Organic Chemicals Co. Ltd., Chinese Academy of Sciences (Chengdu, China). FMN (high-performance liquid chromatography grade) was purchased from Chengdu Ruifensi Biological Technology Co. Ltd., (Chengdu, China). Dulbecco's Modified Eagle's Medium (DMEM), RPMI 1640 medium, and fetal bovine serum (FBS) were purchased from Thermo Fisher Scientific (Waltham, MA, USA). Water soluble tetrazolium (WST-1) and a cytotoxicity assay kit were purchased from Shanghai Beyotime Institute of Biotechnology (Shanghai, China). The solvent used was analytical grade, and purified water was produced using a Millipore water purification system.

Cell culture conditions

HeLa and 3T3 cells were purchased from the American Type Culture Collection (Manassas, VA, USA). The 3T3 cells were cultured in high-glucose DMEM supplemented with 10% FBS and maintained under 5% CO_2 atmosphere at 37°C. HeLa cells were cultured in RPMI 1640 medium supplemented with 10% FBS.

Preparation of drug-loaded MWCNT-COOH

MWCNT-COOH can bind aromatic molecules through π–π stacking because of their ultra-high surface area (Figure 1). FMN loading into the MWCNT-COOH was performed in accordance with a reported method in the literature.[24] FMN was dissolved in methanol and mixed with MWCNT-COOH at the ratio of 1:2 (w/w), followed by sonication for 10 minutes with 3 seconds intervals using an ultrasonic probe sonicator. After that, the mixtures were centrifuged at 10,000 rpm for 10 minutes, and the clear supernatant was measured using UV-visible spectroscopy at 249 nm. The excess of FMN was removed by washing with methanol. The product was finally dried at 50°C in an

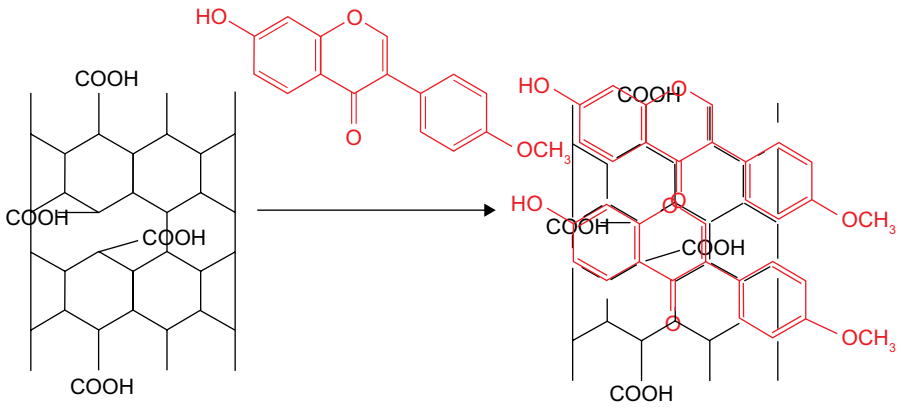

Figure 1 The schematic representation of the possible interaction of FMN with MWCNT-COOH.
Abbreviations: FMN, formononetin; MWCNT-COOH, carboxylic group-functionalized multiwalled carbon nanotubes.

oven to achieve MWCNT-FMN. The calculation equations are as follows:

$$\%\ \text{entrapment efficiency} = \frac{\text{Weight of entrapped FMN in conjugate}}{\text{Weight of original FMN}} \times 100\%$$

$$\%\ \text{loading capacity} = \frac{\text{Weight of entrapped FMN in conjugate}}{\text{Weight of conjugate}} \times 100\%$$

Characterization of MWCNT-FMN

Particle size distribution and zeta potential

The particle size, polydispersity index (PI), and zeta potential of the samples were measured using a Delsa Nano S Particle Analyzer (Beckman Coulter, Brea, CA, USA). The sample was dispersed in ultra-pure deionized water and sonicated for 15 minutes in a water bath sonicator for a proper dispersion of the studied samples. The average value of three repeated scanning was reported as the final result for the test samples.

FTIR

FTIR was used to analyze the chemical structure of the prepared samples. A trace amount of sample was mixed with 95–105 mg potassium bromide and pressed to a pellet. The FTIR spectra were obtained using a FTIR spectrometer (Spectrum 100) in the 400–4,000 cm^{-1} region.

XRD

The MWCNT-COOH, MWCNT-FMN, and FMN samples were measured using XRD (D/max-IIIA, Cu, Kα, λ=1.5406 Å; Rigaku Corporation, Tokyo, Japan), and scans were performed with a step width of 0.02° per step in the 2θ range from 3° to 50°.

DSC

The studies were performed on a DSC thermal analyzer (DSC 4000; PerkinElmer, Waltham, MA, USA). The apparatus was calibrated for temperature by melting a high purity medium. The instrument was flushed with nitrogen. Experiments were run over the temperature range from 25°C to 277°C, with a heating rate of 10°C/min.

SEM

SEM was used to visualize the surface morphology and particle size of the samples to investigate whether the drug-containing CNTs, synthesized as described above, could be examined for the presence of drug crystals. Samples were prepared by making a film on aluminum to a thickness of 200–500 Å under an argon atmosphere using a gold sputter module in a high vacuum evaporator. The coated samples were scanned and photographs were taken using a scanning electron microscope (LEO 1430VP; Zeiss, Oberkochen, Germany).

In vitro drug release

The release behavior of FMN from MWCNT-FMN was carried out in PBS solution (pH 7.4 or 5.3). Briefly, 3 mg MWCNT-FMN and 4 mL of PBS was placed in a dialysis bag (MWCO =8,000–14,000), hermetically tied at both ends and immediately submerged into 20 mL of PBS diffusion medium with constant stirring at 37°C. At timed intervals, the solution was withdrawn and determined by UV–Vis spectroscopy at 249 nm.

Cell viability assay

The in vitro cytotoxicity studies were performed using a WST-1 assay. The procedures for the WST-1 assay have been previously described by Li et al.[25] HeLa and 3T3 cells were inoculated in 96-well plates at a density of 1×10^4 cells/well. The cell suspension (100 µL) was added to the wells in triplicate and incubated overnight for cell attachment. Then, cells in the logarithmic growth phase were exposed to different concentrations of free FMN, MWCNT-COOH, and MWCNT-FMN ranging from 3.13 to 100 µmol/L. The FMN or formulations were diluted in phosphate buffer solution (pH =7.4) prior to addition. After a 48-hour incubation, the supernatant from each well was replaced with 90 µL of new culture media and 10 µL of WST-1, and the plates were further incubated for 4 hours. Subsequently, 90 µL of supernatant from each well was carefully removed to another new 96-well microculture plate, and absorbance at 450 and 630 nm (reference wavelength) was recorded. Background and negative controls were obtained by measuring the culture medium and untreated cell medium, respectively. The data obtained were averaged and processed using the following equation to calculate the percentage cell viability. The concentration that inhibits 50% of the cellular growth (IC_{50}) was calculated from the cell viability data as the drug concentration in which cell growth was inhibited by 50%.

$$\text{Cell viability (\%)} = \frac{\text{Average}_{\text{test}}}{\text{Average}_{\text{control}}} \times 100\%$$

Apoptosis assay by AO/EB staining method

The apoptosis assessment was performed using a staining method by acridine orange and ethidium bromide (AO/EB). 3T3 cells and HeLa cells were plated on 12-well plates at a density of 1×10^4 cells/well and the cells were incubated with FMN and MWCNT-FMN for 24 hours by using different concentrations (35 and 70 µmol/L for HeLa cells, and 70 µmol/L for 3T3 cells). The cells were washed with ice-cold PBS and then exposed to AO/EB (AO: 50 µg/mL, EB: 50 µg/mL) for 30 minutes. After being rinsed twice with ice-cold PBS, the cells were observed under fluorescence microscope.

In vitro detection of ROS

The intracellular content of ROS was detected using the 2′,7′-dichlorodihydrofluorescein diacetate (DCHF-DA) probe. 3T3 cells and HeLa cells were seeded into 12-well plates at a density of 1×10^4 cells/well, and the cells were incubated with FMN and MWCNT-FMN for 24 hours by using different concentrations (35 and 70 µmol/L for HeLa cells, and 70 µmol/L for 3T3 cells). DCHF-DA was then added in the plates and incubated at 37°C for 30 minutes in the dark. The treated cells were washed with ice-cold PBS twice and then imaged under a fluorescent microscope.

MMP assay

MMP was determined using 5,5′,6,6′-tetrachloro-1,1′,3,3′-tetraethyl-imidacarbocyanine iodide (JC-1) dye. 3T3 cells and HeLa cells were incubated with FMN and MWCNT-FMN for 24 hours by using different concentrations (35 and 70 µmol/L for HeLa cells, and 70 µmol/L for 3T3 cells). Cells were washed three times with ice-cold PBS and incubated with JC-1 at 37°C for 30 minutes in the dark. Then the cells were rinsed again and imaged by fluorescence microscopy.

Statistical analysis

All data are shown as the mean ± standard deviation (SD) of three separate experiments. One-way ANOVA was used to analyze the differences between the two treatment groups. Differences were considered to be significant at $P<0.05$ and extremely significant at $P<0.01$.

Results and discussion

Drug loading study

The concentration of unconjugated FMN was determined using a UV–visible spectrophotometer at 249 nm, which is the characteristic absorption wavelength of FMN. The entrapment efficiency of MWCNT-FMN was 28.77%±0.15% and the loading capacity was 12.05%±0.20%.

Characterization of drug-loaded MWCNT-COOH

Particle size distribution and zeta potential studies

The average size of the MWCNT-COOH was ~176.0±1.1 nm, while the diameter of the MWCNT-FMN was 277.3±3.7 nm (Figure 2A). Similar results have been reported by Sobhani et al,[16] who suggested that there was no significant aggregation of MWCNT-COOH after their loading with hydrophobic drug. The PI for the MWCNT-COOH before and after loading with FMN was 0.275±0.003 and 0.281±0.024, respectively. These findings might be attributable to the nonsymmetric nature of the CNTs. The obtained PI values were <0.4, indicating the reliability of the reported size values as well as some homogeneity.[26] The zeta potential of the MWCNT-COOH and MWCNT-FMN was –27.08±2.33 mV and –27.15±1.15 mV (Figure 2B), respectively, which indicated that the prepared composites were relatively stable.

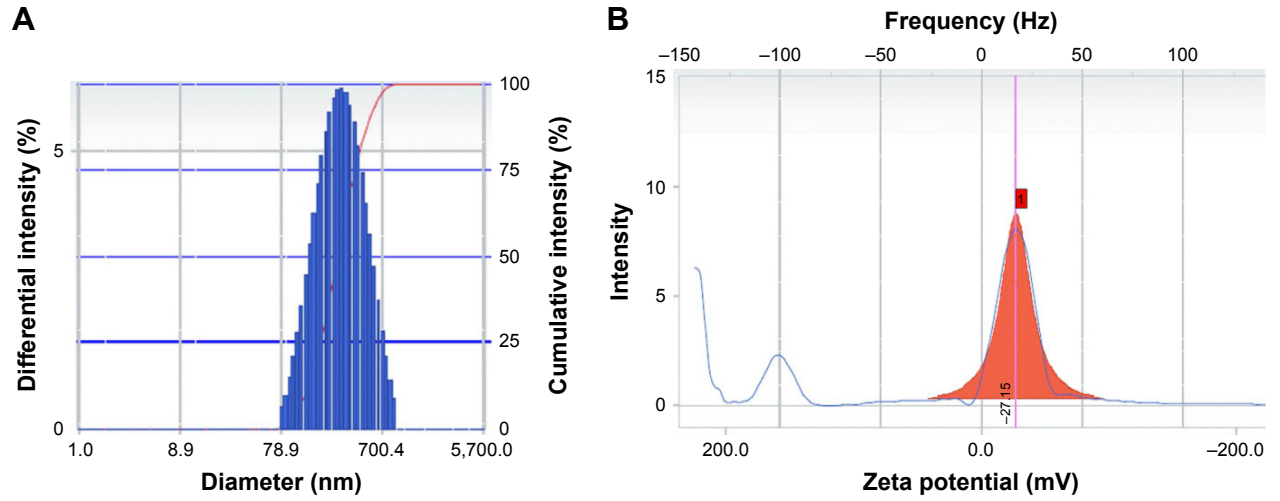

Figure 2 Spectra of particle size distribution (**A**) and zeta potential (**B**) for MWCNT-FMN.
Abbreviation: MWCNT-FMN, multiwalled carbon nanotube–formononetin.

FTIR analysis

The FTIR spectra of the MWCNT-COOH and MWCNT-FMN are illustrated in Figure 3A. They had similar characteristic peaks at ~3,424 and 1,628 cm^{-1}, which was attributed to –OH and C=O stretching bands from the hydrophilic carboxyl (–COOH) groups attached to the MWCNT. The FTIR spectrum of FMN shows characteristic absorption peaks at 1,608, 1,569, and 1,513 cm^{-1}, which can be attributed to the skeleton vibration of the aromatic compound, which belongs to the isoflavone group. Those peaks disappeared in the spectra of the MWCNT-FMN. Additionally, the bands at 2,910 cm^{-1} in the spectra of the MWCNT-FMN may be caused by the C–H stretching vibrations from the methyl functional groups of FMN, suggesting that the drug was successfully loaded into the MWCNT-COOH.

XRD analysis

XRD is a surface-sensitive quantitative spectroscopic technique that can be used to investigate the composition of samples. Figure 3B shows that pure MWCNT-COOH and MWCNT-FMN exhibited diffraction peaks in the range of ~25°–30°, which was assigned to the hexagonal graphite structure.[27] The spectrum of FMN showed numerous distinct peaks at 2θ of 7.4°, 9.8°, 14.86°, 16.2°, 22.4°, and 25.86°, indicating that FMN was a highly crystalline drug. The diffraction peaks of the drug could not be detected in the MWCNT-FMN. This implied that FMN transformed from crystalline to an amorphous state in the conjugates and that the carbon graphitic crystallite structure of the MWCNT-COOH was not affected by the drug loading process. A similar phenomenon can be seen in other works.[28,29]

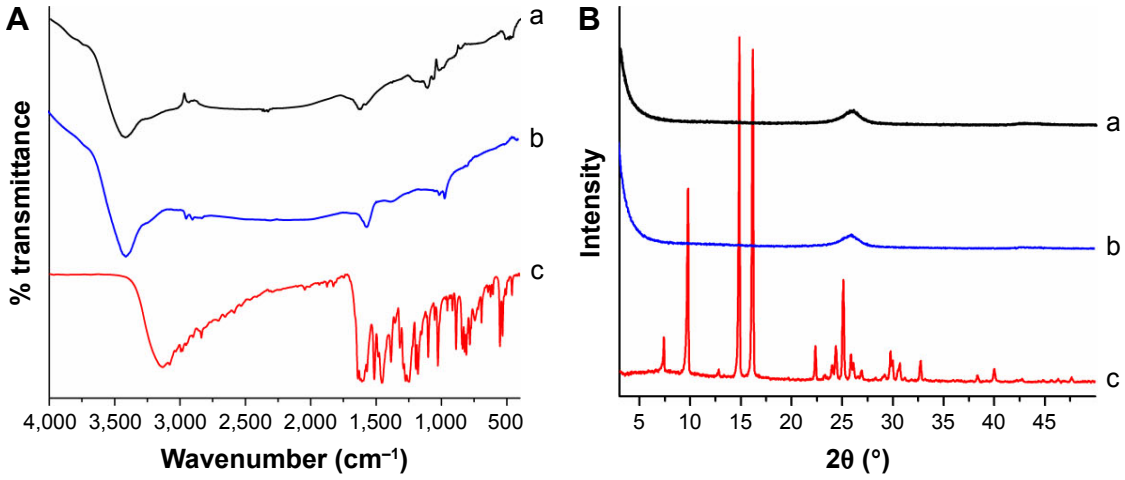

Figure 3 (**A**) FTIR spectra and (**B**) XRD patterns of MWCNT-COOH (a), MWCNT-FMN (b), and FMN (c).
Abbreviations: FTIR, Fourier transform infrared spectrometry; MWCNT-COOH, carboxylic group-functionalized multiwalled carbon nanotubes; MWCNT-FMN, multiwalled carbon nanotube–formononetin; XRD, X-ray diffractometry.

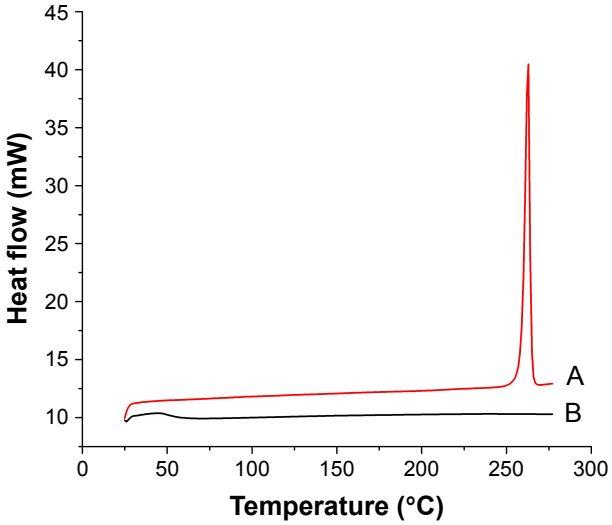

Figure 4 DSC of FMN (A) and MWCNT-FMN (B).
Abbreviations: DSC, differential scanning calorimetry; FMN, formononetin; MWCNT-FMN, multiwalled carbon nanotube–formononetin.

DSC analysis

As shown in Figure 4, the phase transition of FMN happened from 250.4°C to 269.8°C, and a fusion endothermic peak could be seen at 262.73°C (ΔH =0.147 kJ/mol). This is because the free form of FMN is in the crystalline state in nature. This melting peak was not present in the DSC thermogram of the MWCNT-FMN conjugates, indicating that FMN in the conjugates was no longer present in a crystalline form but was converted into an amorphous state.

SEM analysis

The microstructures of the MWCNT-COOH before and after loading with FMN were characterized using SEM imaging, as shown in Figure 5. Figure 5A demonstrates that FMN had a sheet crystalline structure. Figure 5B shows that the surface of the aggregated MWCNT-COOH had a number of intertwined tubes, while the surface of the MWCNT-FMN conjugates was smoother (Figure 5C and D). By comparing Figure 5A with Figure 5C and D, it was found that there were many filaments that could be observed in Figure 5A, which almost disappeared in Figure 5C and D, suggesting that the MWCNT-COOH was covered with FMN in a high density and agglomeration manner. The images resemble an SEM image of MWCNT/glassy carbon electrode that Liu et al have reported.[30] Accordingly, this provides further proof that the drug is adsorbed onto the CNTs.

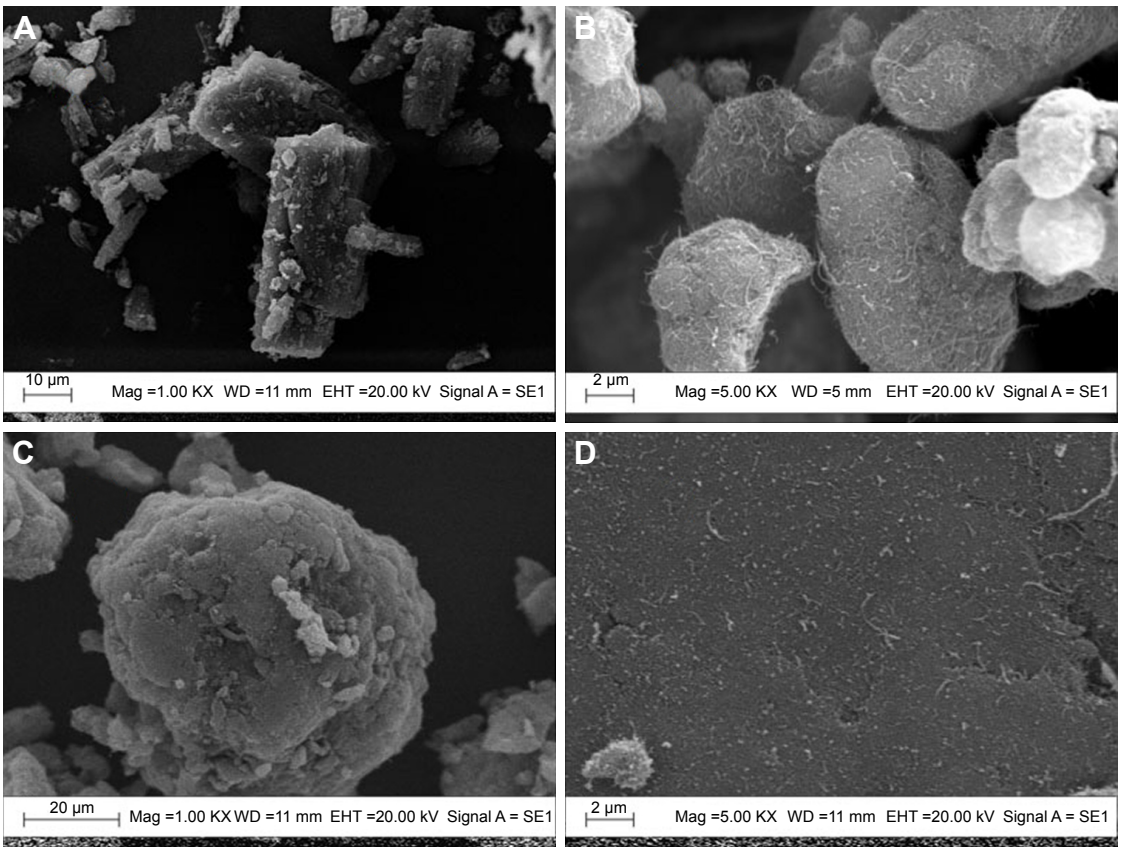

Figure 5 SEM images of FMN (**A**), MWCNT-COOH (**B**), and MWCNT-FMN with different magnifications (**C**, **D**).
Abbreviations: SEM, scanning electron microscopy; FMN, formononetin; MWCNT-COOH, carboxylic group-functionalized multiwalled carbon nanotubes; MWCNT-FMN, multiwalled carbon nanotubes–formononetin.

In vitro release

As shown in Figure 6, the release pattern was as follows: the samples achieved burst release in the initial stage followed by sustained release. The release rate of FMN from MWCNT-FMN was significantly lower than that from FMN solution at pH 5.3 and 7.4, which could be the result of the loaded drug encountering steric hindrance on the ends and sidewalls of MWCNT-COOH.[31] pH value is one of the most important factors for studying the drug release process.[9] In this study, the release profile of MWCNT-FMN in PBS solution at pH 7.4 and 5.3 was investigated. The cumulative release rate of MWCNT-FMN reached 52.20%±1.91% within 48 hours at pH 7.4 compared with 16.38%±2.99% at pH 5.3, which could be caused by the increased solubility of FMN in aqueous solution of increasing pH values. Consequently, the π–π stacking interaction and hydrogen bonding interaction between FMN and MWCNT-COOH maybe weakened accordingly.

In vitro cytotoxicity

To assess the biocompatibility and pharmacological activity of the free FMN, and the MWCNT-COOH before and after loading with FMN, in vitro cytotoxicity studies were conducted on 3T3 and HeLa cells using the WST-1 reagent. WST-1 is reduced by cellular mitochondrial dehydrogenases to water-soluble formazan. The more cells proliferate, the darker the color gets, while the greater the cytotoxicity is, the lighter the color gets. It has been reported that the use of MTT to detect the cytotoxicity of CNTs will reduce the survival rate of the tested cells to produce a false positive;[32] hence, the WST-1 method was used in this experiment to detect cytotoxicity. Figure 7 shows that the increased concentration of treated samples had no significant effect on the inhibition of proliferation and viability for normal cells (3T3 cells) within the concentration range from 3.13 to 100 μmol/L. The cytotoxic effect of MWCNT-FMN on the 3T3 cell lines may be caused by the nanotubes having an effect on cellular protein content. Additionally, the nanotubes resulted in a less than 20% loss of viable 3T3 cells after 48 hours, which could be associated with the functional groups rendering them more hydrophilic or the MWCNT-COOH having a short length.[33,34] In contrast, tumor cells (HeLa cells) exhibited significant cell growth inhibition when incubated with the above three substances, and the growth inhibition was concentration-dependent. The findings were similar to those reported by Tan et al.[29] For HeLa cells, the IC_{50} of FMN and MWCNT-FMN were (72.995±0.551) μmol/L and (72.112±5.671) μmol/L, respectively. There was no significant difference in the cytotoxicity against HeLa cells between the two samples. It was noted that MWCNT-FMN conjugates produced a much lower cell viability than FMN within the concentration range from 6.25 to 50 μmol/L. The increased cytotoxic response of MWCNT-FMN may possibly be caused by caveolae-mediated endocytosis and specific uptake by cancerous cells causing a dose-dependent cytotoxic response.[31]

Apoptosis assay by AO/EB staining method

AO/EB staining method is commonly used to distinguish the normal cells and apoptotic cells. AO can penetrate the membrane of normal cells while EB only stains cells that have lost

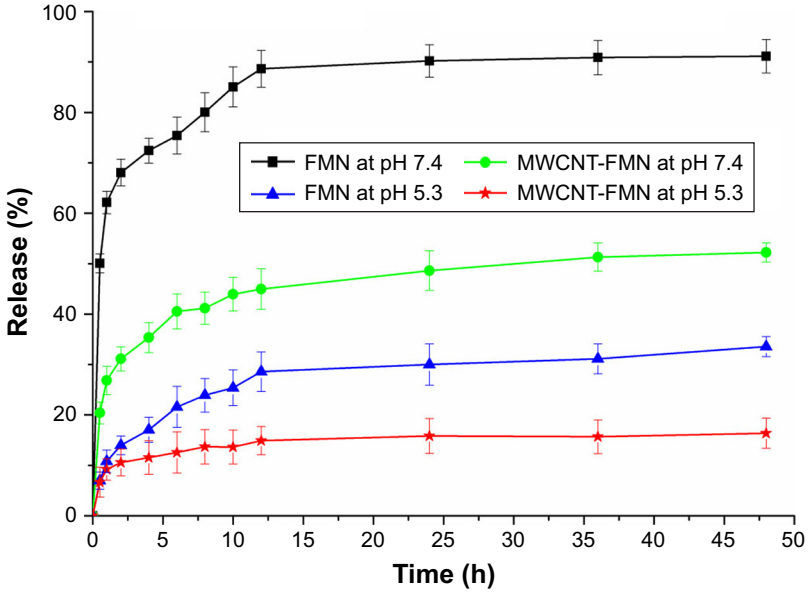

Figure 6 Cumulative FMN release (%) from FMN solution or MWCNT-FMN under different pH conditions.
Abbreviations: FMN, formononetin; MWCNT-FMN, multiwalled carbon nanotubes–formononetin.

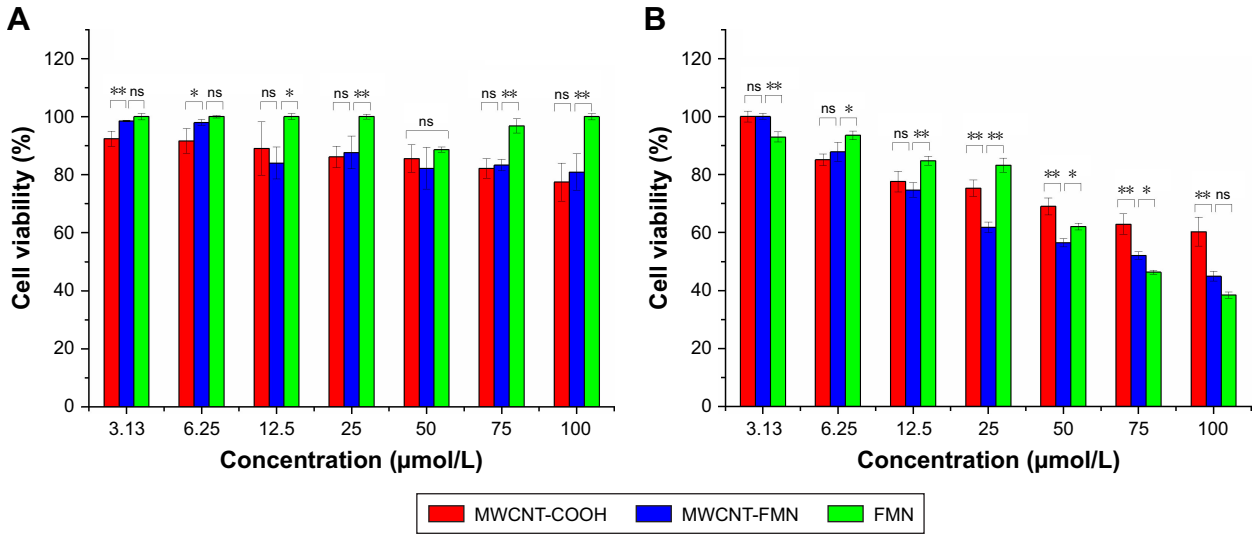

Figure 7 Cell viability of (**A**) 3T3 cells and (**B**) HeLa cells treated with MWCNT-COOH, MWCNT-FMN, and FMN was tested by WST-1 assay at series of concentrations after 48 hours.
Notes: The data are mean ± SD of triplicate experiments (n=3). ns: not significant; *significant; **extremely significant.
Abbreviations: MWCNT-COOH, carboxylic group-functionalized multiwalled carbon nanotubes; MWCNT-FMN, multiwalled carbon nanotube–formononetin; FMN, formononetin; WST-1, water soluble tetrazolium; SD, standard deviation.

membrane integrity. The morphological changes can be seen in Figure 8. The FMN and MWCNT-FMN exhibited similar phenomenon as that of blank control (the cells treated with PBS) in 3T3 cells (Figure 8Aa–c). In contrast, in HeLa cells, the blank control (Figure 8Ba) exhibited normal shape with faint green fluorescence. After being treated with 35 μmol/L of FMN and MWCNT-FMN for 24 hours (Figure 8Bb and d, respectively), the cells showed stronger fluorescence signal

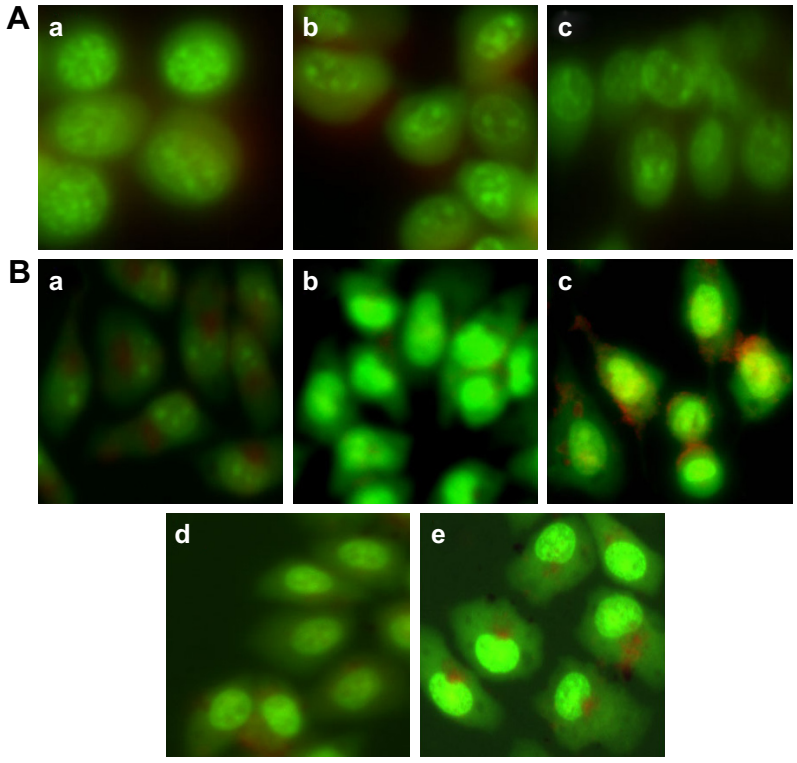

Figure 8 The apoptosis of (**A**) 3T3 and (**B**) HeLa cells treated with different samples: (**A**-a) blank control, (**A**-b) 70 μmol/L of FMN, and (**A**-c) 70 μmol/L of MWCNT-FMN; (**B**-a) blank control, (**B**-b, **B**-c) 35 and 70 μmol/L of FMN, and (**B**-d, **B**-e) 35 and 70 μmol/L of MWCNT-FMN.
Note: Magnification for the figures is 200×.
Abbreviations: FMN, formononetin; MWCNT-FMN, multiwalled carbon nanotubes–formononetin.

compared with the control group, and the basic characteristics of apoptotic cells such as chromatin condensation and nuclear shrinkage were observed. With increasing concentrations of FMN and MWCNT-FMN from 35 to 70 μmol/L (Figure 8Bc and e, respectively), the green fluorescence continued to be concentrated in the nuclei owing to the nuclear shrinkage and the red fluorescence became more obvious due to the lack of membrane integrity, which implied that the FMN and MWCNT-FMN of 70 μmol/L could trigger apoptosis, including early apoptosis and late apoptosis.[35] The results of the present study suggested that MWCNT-FMN could induce apoptosis in HeLa cells.

Detection of ROS level

Many reports indicated that the intracellular ROS content was involved with cellular senescence and apoptosis.[36,37] The antioxidase in the tumor cells would reach their maximum tolerance to ROS with the increase of ROS content in cells as the result of cellular apoptosis. The ROS level was detected using DCFH-DA fluorescent probe. It could be cleaved by intracellular esterases into its nonfluorescent form (DCFH). Then DCFH was oxidized by intracellular free radicals to produce a fluorescent product (DCF). As shown in Figure 9Aa–c, the FMN and MWCNT-FMN exhibited the similar phenomenon compared with the blank control (the cells treated with PBS) in 3T3 cells. In HeLa cells, no obvious fluorescent image could be detected in the control (Figure 9Ba). Contrarily, the fluorescent image could be observed after the treatment of HeLa cells with Rosup (positive control) (Figure 9Bb), FMN (Figure 9Bc), and MWCNT-FMN (Figure 9Be) at the concentration of 35 μmol/L for 24 hours. Obviously, compared with FMN, MWCNT-FMN induced greater rates of ROS generation. Moreover, as the concentrations of FMN and MWCNT-FMN were increased by 70 μmol/L, it was clearly found that the fluorescence of DCF continues to be intensive and the intensity of HeLa cells exposed to 70 μmol/L MWCNT-FMN was remarkably elevated in comparison with the Rosup-treated cells (Figure 9Bd and f). The results indicated that FMN and MWCNT-FMN could significantly enhance the ROS level of HeLa cells. And MWCNT-FMN expressed more cytotoxicity than FMN.

Detection of MMP

Decrease of MMP was one of the signs of cellular apoptosis, and JC-1 was a membrane potential–sensitive fluorescent probe that could detect the level of membrane potential. The high membrane potential could promote JC-1 aggregated in

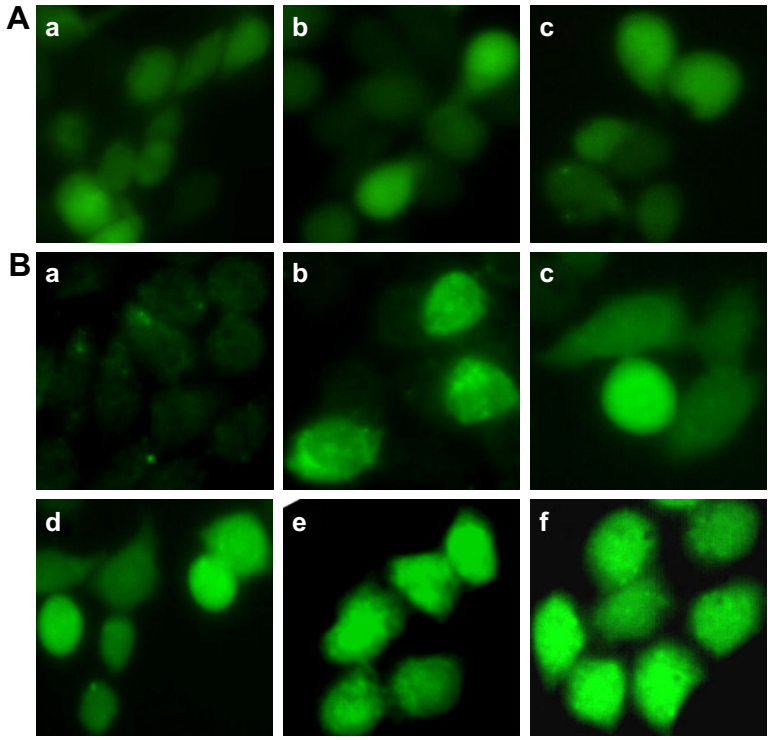

Figure 9 The ROS generation in (**A**) 3T3 cells and (**B**) HeLa cells exposed to different samples: (**A**-a) blank control, (**A**-b) 70 μmol/L of FMN, and (**A**-c) 70 μmol/L of MWCNT-FMN; (**B**-a) blank control, (**B**-b) positive control, (**B**-c, d) 35 and 70 μmol/L of FMN, (**B**-e, f) 35 and 70 μmol/L of MWCNT-FMN.
Note: Magnification for the figures is 200×.
Abbreviations: ROS, reactive oxygen species; FMN, formononetin; MWCNT-FMN, multiwalled carbon nanotube–formononetin.

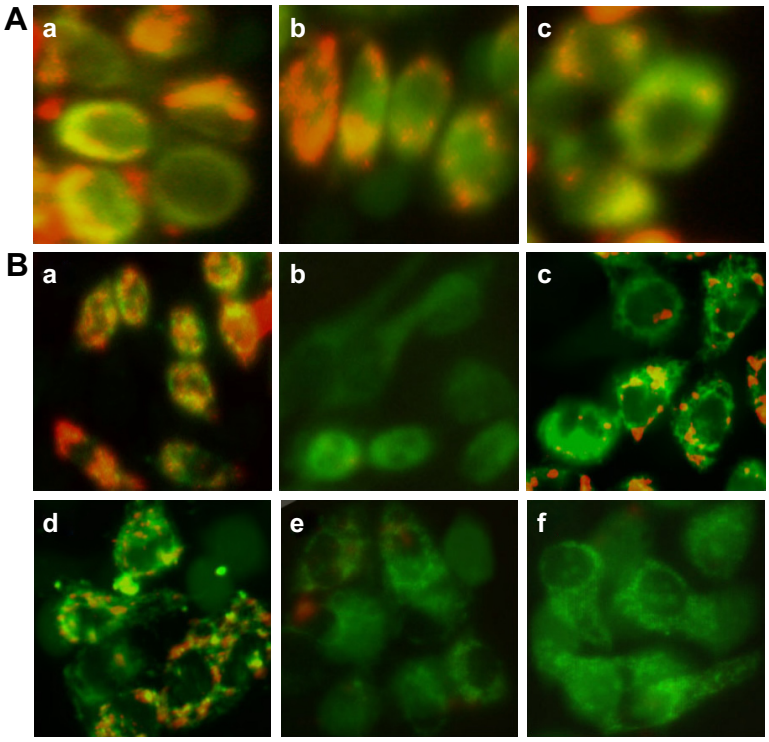

Figure 10 The MMP of (**A**) 3T3 cells and (**B**) HeLa cells exposed to different samples: (**A**-a) blank control, (**A**-b) 70 μmol/L of FMN, and (**A**-c) 70 μmol/L of MWCNT-FMN; (**B**-a) blank control, (**B**-b) positive control, (**B**-c, d) 35 and 70 μmol/L of FMN, (**B**-e, f) 35 and 70 μmol/L of MWCNT-FMN.
Note: Magnification for the figures is 200×.
Abbreviations: MMP, mitochondrial membrane potential; FMN, formononetin; MWCNT-FMN, multiwalled carbon nanotube–formononetin.

matrix to present red fluorescence, while low potential prevented from aggregation and present green fluorescence.[38] As shown in Figure 10Aa, 3T3 cells exhibited strong red fluorescence in the control, and the FMN (Figure 10Ab) and MWCNT-FMN (Figure 10Ac) exhibited similar phenomenon compared with the blank control. Figure 10Ba shows that HeLa cells exhibited strong red fluorescence in the control; by contrast, HeLa cells mainly emitted green fluorescence after the cells were exposed to CCCP (carbonyl cyanide m-chlorophenyl hydrazone, positive control) (Figure 10Bb), FMN, and MWCNT-FMN. In addition, as shown in Figure 10Bc and e, the fluorescence intensity ratio of red/green for the cells that were treated with 35 μmol/L MWCNT-FMN was smaller than that of the cells treated with 35 μmol/L of FMN. Similarly, with increasing concentration in the MWCNT-FMN-treated group, the green fluorescence was increased while the red fluorescence was dissipated. The phenomenon was more evident than that of the FMN-treated group (Figure 10Bd and f). Therefore, the membrane potential of cells treated with MWCNT-FMN was lower than that of cells treated with FMN. Compared with FMN, MWCNT-FMN was more cytotoxic against HeLa cells. These findings also demonstrated that both FMN and MWCNT-FMN could induce a decrease of MMP of HeLa cells corresponding to cellular apoptosis.

Conclusion

In summary, the current study demonstrated that MWCNT-COOH was an optimal FMN carrier. The entrapment efficiency of MWCNT-FMN was 28.77%±0.15% and the loading capacity was 12.05%±0.20%. The MWCNT-FMN showed a pH-responsive release behavior, and the release rate of FMN was significantly higher than that of MWCNT-FMN at pH 7.4 and 5.3. As a result of the WST-1 assay, increasing the concentration of the samples did not significantly change their toxicity in 3T3 cells. Similarly, the FMN and MWCNT-FMN did not induce significant apoptotic morphology, ROS overload, or collapse of MMP in 3T3 cells. Yet FMN, MWCNT-COOH, and MWCNT-FMN exhibited enhanced anticancer activity against HeLa cell lines in a dose-dependent manner. AO/EB-stained cells revealed that MWCNT-FMN could effectively induce the change of apoptotic morphology of HeLa cells, and the conjugates could enhance the level of ROS and induce the decrease of MMP. Previous reports have revealed that ROS may play a vital role in the decrease of MMP in cells.[37] Depolarization of MMP is an important step in the apoptotic process and is lethal to the cells, which could cause the release of diverse apoptogenic factors from mitochondria into cytoplasm.[39]

In conclusion, we have successfully prepared the MWCNT-FMN and preliminarily found that the MWCNT-FMN

may induce the apoptosis of HeLa cells through ROS-mediated mitochondrial dysfunction pathway.

Acknowledgment

This work was financially supported by the National Nature Science Foundation of China (number 81403111).

Disclosure

The authors report no conflicts of interest in this work.

References

1. Li T, Zhao X, Mo Z, et al. Formononetin promotes cell cycle arrest via downregulation of Akt/Cyclin D1/CDK4 in human prostate cancer cells. *Cell Physiol Biochem*. 2014;34(4):1351–1358.
2. Zhou R, Xu L, Ye M, et al. Formononetin inhibits migration and invasion of MDA-MB-231 and 4T1 breast cancer cells by suppressing MMP-2 and MMP-9 through PI3K/AKT signaling pathways. *Horm Metab Res*. 2014;46(11):753–760.
3. Zhang X, Bi L, Ye Y, Chen J. Formononetin induces apoptosis in PC-3 prostate cancer cells through enhancing the Bax/Bcl-2 ratios and regulating the p38/Akt pathway. *Nutr Cancer*. 2014;66(4):656–661.
4. Yang Y, Zhao Y, Ai X, Cheng B, Lu S, Xh A. Formononetin suppresses the proliferation of human non-small cell lung cancer through induction of cell cycle arrest and apoptosis. *Int J Clin Exp Pathol*. 2014;7(12):8453–8461.
5. Huh JE, Lee WI, Kang JW, et al. Formononetin attenuates osteoclastogenesis via suppressing the RANKL-induced activation of NF-κB, c-Fos, and nuclear factor of activated T-cells cytoplasmic 1 signaling pathway. *J Nat Prod*. 2014;77(11):2423–2431.
6. Zhou GW, Mu H, Li YF, Yang Y. A new method in determination of formononetin content in trifolium pratense. *Zhong Yao Cai*. 2007;30(1):53–56.
7. Iijima S. Helical microtubules of graphitic carbon. *Nature*. 1991;354(6348):56–58.
8. Ali-Boucetta H, Al-Jamal KT, Mccarthy D, et al. Multiwalled carbon nanotube-doxorubicin supramolecular complexes for cancer therapeutics. *Chem Commun*. 2008;28(4):459–461.
9. Yu B, Tan L, Zheng R, Tan H, Zheng L. Targeted delivery and controlled release of Paclitaxel for the treatment of lung cancer using single-walled carbon nanotubes. *Mater Sci Eng C Mater Biol Appl*. 2016;68:579–584.
10. Kam NW, O'Connell M, Wisdom JA, Dai H. Carbon nanotubes as multifunctional biological transporters and near-infrared agents for selective cancer cell destruction. *Proc Natl Acad Sci U S A*. 2005;102(33):11600–11605.
11. Mehra NK, Jain K, Jain NK. Pharmaceutical and biomedical applications of surface engineered carbon nanotubes. *Drug Discov Today*. 2015;20(6):750–759.
12. Tian Z, Yin M, Ma H, et al. Supramolecular assembly and antitumor activity of multiwalled carbon nanotube-camptothecin complexes. *J Nanosci Nanotechnol*. 2011;11(2):953–958.
13. Liu Z, Tabakman SM, Chen Z, Dai H. Preparation of carbon nanotube bioconjugates for biomedical applications. *Nat Protoc*. 2009;4(9):1372–1381.
14. Datir SR, Das M, Singh RP, Jain S. Hyaluronate tethered, "smart" multiwalled carbon nanotubes for tumor-targeted delivery of doxorubicin. *Bioconjug Chem*. 2012;23(11):2201–2213.
15. Xu Y, Wang J, Hu JP, et al. Purification of multi-walled carbon nanotubes and its surface modification. *Sciencepaper Online*. 2010;5(6):423–426.
16. Sobhani Z, Dinarvand R, Atyabi F, Ghahremani M, Adeli M. Increased paclitaxel cytotoxicity against cancer cell lines using a novel functionalized carbon nanotube. *Int J Nanomedicine*. 2011;6:705–719.
17. Liu Z, Tabakman S, Welsher K, Dai H. Carbon nanotubes in biology and medicine: in vitro and in vivo detection, imaging and drug delivery. *Nano Res*. 2009;2(2):85–120.
18. Ren J, Shen S, Wang D, et al. The targeted delivery of anticancer drugs to brain glioma by PEGylated oxidized multi-walled carbon nanotubes modified with angiopep-2. *Biomaterials*. 2012;33(11):3324–3333.
19. Razzazan A, Atyabi F, Kazemi B, Dinarvand R. In vivo drug delivery of gemcitabine with PEGylated single-walled carbon nanotubes. *Mater Sci Eng C Mater Biol Appl*. 2016;62:614–625.
20. Foldvari M, Bagonluri M. Carbon nanotubes as functional excipients for nanomedicines: I. Pharmaceutical properties. *Nanomedicine*. 2008;4(3):173–182.
21. Foldvari M, Bagonluri M. Carbon nanotubes as functional excipients for nanomedicines: II. Drug delivery and biocompatibility issues. *Nanomedicine*. 2008;4(3):183–200.
22. Wang X, Liu Z. Carbon nanotubes in biology and medicine: an overview. *Chin Sci Bull*. 2012;57(2–3):167–180.
23. Wong BS, Yoong SL, Jagusiak A, et al. Carbon nanotubes for delivery of small molecule drugs. *Adv Drug Deliv Rev*. 2013;65(15):1964–2015.
24. Zhang YY, Fu XD, Liu KD, et al. Preparation and tumor targeting of NGR-SWCNTs-Paclitaxel. *J Chin Pharm*. 2013;48(120):1748–1754.
25. Li R, Feng F, Wang Y, et al. Folic acid-conjugated pH/temperature/redox multi-stimuli responsive polymer microspheres for delivery of anti-cancer drug. *J Colloid Interface Sci*. 2014;429:34–44.
26. Raza K, Kumar D, Kiran C, et al. Conjugation of docetaxel with multiwalled carbon nanotubes and codelivery with piperine: implications on pharmacokinetic profile and anticancer activity. *Mol Pharm*. 2016;13(7):2423–2432.
27. Nawaz MA, Rauf S, Catanante G, et al. One step assembly of thin films of carbon nanotubes on screen printed interface for electrochemical aptasensing of breast cancer biomarker. *Sensors*. 2016;16(10):pii:E1651.
28. Moribe K, Makishima T, Higashi K, et al. Encapsulation of poorly water-soluble drugs into organic nanotubes for improving drug dissolution. *Int J Pharm*. 2014;469(1):190–196.
29. Tan JM, Karthivashan G, Arulselvan P, Fakurazi S, Hussein MZ. Characterization and in vitro studies of the anticancer effect of oxidized carbon nanotubes functionalized with betulinic acid. *Drug Des Devel Ther*. 2014;8:2333–2343.
30. Liu Y, Liu X, Liu Y, et al. Construction of a highly sensitive non-enzymatic sensor for superoxide anion radical detection from living cells. *Biosens Bioelectron*. 2017;90:39–45.
31. Mehra NK, Jain NK. Development, characterization and cancer targeting potential of surface engineered carbon nanotubes. *J Drug Target*. 2013;21(8):745–758.
32. Wörle-Knirsch JM, Pulskamp K, Krug HF. Oops they did it again! Carbon nanotubes hoax scientists in viability assays. *Nano Lett*. 2006;6(6):1261–1268.
33. Jos A, Pichardo S, Puerto M, et al. Cytotoxicity of carboxylic acid functionalized single wall carbon nanotubes on the human intestinal cell line Caco-2. *Toxicol In Vitro*. 2009;23(8):1491–1496.
34. Sayes CM, Liang F, Hudson JL, et al. Functionalization density dependence of single-walled carbon nanotubes cytotoxicity in vitro. *Toxicol Lett*. 2006;161(2):135–142.
35. Wasim L, Chopra M. Synergistic anticancer effect of panobinostat and topoisomerase inhibitors through ROS generation and intrinsic apoptotic pathway induction in cervical cancer cells. *Cell Oncol*. 2018;41(2):201–212.
36. Kim SW, Kyung Lee Y, Yeon Lee J, Hee Hong J, Khang D. PEGylated anticancer-carbon nanotubes complex targeting mitochondria of lung cancer cells. *Nanotechnology*. 2017;28(46):465102.
37. Jiang GB, Zheng X, Yao JH, et al. Ruthenium(II) polypyridyl complexes induce BEL-7402 cell apoptosis by ROS-mediated mitochondrial pathway. *J Inorg Biochem*. 2014;141:170–179.
38. Kodali VK, Roberts JR, Shoeb M, et al. Acute in vitro and in vivo toxicity of a commercial grade boron nitride nanotube mixture. *Nanotoxicology*. 2017;11(8):1040–1058.
39. Rayman MP. Selenium in cancer prevention: a review of the evidence and mechanism of action. *Proc Nutr Soc*. 2005;64(4):527–542.